Published in final edited form as:

Biomaterials. 2017 June ; 128: 44–55. doi:10.1016/j.biomaterials.2017.03.005.

A microengineered collagen scaffold for generating a polarized crypt-villus architecture of human small intestinal epithelium

Yuli Wang[a], **Dulan B. Gunasekara**[a], **Mark I. Reed**[a], **Matthew DiSalvo**[b], **Scott J. Bultman**[c], **Christopher E. Sims**[a], **Scott T. Magness**[b], and **Nancy L. Allbritton**[a,b,*]

[a]Department of Chemistry, University of North Carolina, Chapel Hill, NC 27599, USA

[b]Department of Biomedical Engineering, University of North Carolina, Chapel Hill, NC 27599, USA and North Carolina State University, Raleigh, NC 27607, USA

[c]Department of Genetics, University of North Carolina, Chapel Hill, NC 27599, USA

Abstract

The human small intestinal epithelium possesses a distinct crypt-villus architecture and tissue polarity in which proliferative cells reside inside crypts while differentiated cells are localized to the villi. Indirect evidence has shown that the processes of differentiation and migration are driven in part by biochemical gradients of factors that specify the polarity of these cellular compartments; however, direct evidence for gradient-driven patterning of this *in vivo* architecture has been hampered by limitations of the *in vitro* systems available. Enteroid cultures are a powerful *in vitro* system; nevertheless, these spheroidal structures fail to replicate the architecture and lineage compartmentalization found *in vivo*, and are not easily subjected to gradients of growth factors. In the current work, we report the development of a micropatterned collagen scaffold with suitable extracellular matrix and stiffness to generate an *in vitro* self-renewing human small intestinal epithelium that replicates key features of the *in vivo* small intestine: a crypt-villus architecture with appropriate cell-lineage compartmentalization and an open and accessible luminal surface. Chemical gradients applied to the crypt-villus axis promoted the creation of a stem/progenitor-cell zone and supported cell migration along the crypt-villus axis. This new approach combining microengineered scaffolds, biophysical cues and chemical gradients to control the intestinal epithelium *ex vivo* can serve as a physiologically relevant mimic of the human small intestinal

*Corresponding author. nlallbri@unc.edu (N.L. Allbritton).

Conflict of interest

N.L.A., Y.W., C.E.S., S.T.M., S.J.B. have a financial interest in Altis Biosystems LLC. The following authors declare no conflicts: D.B.G., M.I.R., M.D.

Submission declaration and verification

Work described has not been published previously, that it is not under consideration for publication elsewhere, that its publication is approved by all authors and, if accepted, it will not be published elsewhere in the same form, in English or in any other language, including electronically without the written consent of the copyright-holder.

Author Contributions

Y.W., S.J.B., C.E.S., S.T.M., N.L.A. designed experiments; Y.W., M.D., D.B.G., M.I.R. performed experiments and provided technical support; Y.W., M.D., N.L.A. analyzed data; Y.W. and N.L.A. administered experiments; Y.W., C.E.S., N.L.A. wrote the paper. All authors have approved the final article.

epithelium, and is broadly applicable to model other tissues that rely on gradients for physiological function.

Graphical Abstract

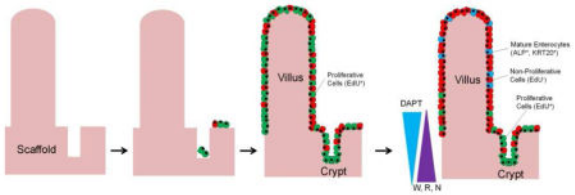

Keywords

scaffold; microfabrication; intestine; stem cell; crypt; villus

1. Introduction

The small intestine is a highly specialized organ that is the major site for digestion and nutrient absorption as well as serving critical roles in oral drug uptake and metabolism, while also being a target of many pathogens and toxins [1]. The lining of the small intestine is a monolayer composed primarily of absorptive enterocytes that are arranged along a microscale topography [2] composed of tightly spaced invaginations (crypts) that are contiguous with larger projections into the intestinal lumen (villi). Stem cells reside in the crypts and proliferate to give rise to differentiated cells that migrate up the crypt-villus axis and cover the villi projections [3]. The microenvironment of the crypt-villus axis, particularly the presence of chemical gradients of growth and morphogens, is believed to play an important role in patterning the polarity of proliferative and differentiated compartments and regulation of proper stem/progenitor cell differentiation of the small intestinal epithelium [4]. It has also been recognized that metabolic factors generated by the gut microbiome form gradients from the lumen to crypt that likely impact development, health and disease of the intestine as well as the organism as a whole [5–8]. Despite a wealth of indirect evidence, the detailed role of various chemical factors and their concentrations within the crypt-villus microenvironment remains poorly understood [9]. Experimental modeling of intestinal epithelial biology and physiology are limited due to the lack of *ex* vivo platforms that mimic key features of the small intestinal epithelium such as distinct stem/progenitor and differentiated cell compartments, forward and reverse gradients of mitogens/morphogens and nutrients, and ordered cellular migration along the crypt-villus axis [10].

Prior to the current age of organoid (or enteroid) technologies [11], *ex vivo* small intestine models were relegated to the use of colon cancer cell lines as no reliable small intestinal transformed cell line exits. With the goal of developing a miniaturized *in vitro* assay platform having the potential to replicate small intestinal form and function, a number of microdevices have been developed, almost all of which incorporate the Caco-2 cancer cell line as the tissue mimic [2, 10, 12–26]. These devices use a variety of techniques to create a

topological representation of the microenvironment. Microscale 3D scaffolds and surface coatings employing extracellular matrices (ECM) have been shown to influence growth properties, differentiation, gene expression and absorptive functions of Caco-2 cells cultured on these devices [2, 12, 13, 19, 21]. To better replicate biomimetic surface properties, a number of different materials have been incorporated into the devices as substrates for cell culture, including hydrogels, PDMS, silk and decellularized porcine intestine [12, 17, 20, 22]. The introduction of dynamic properties such as fluid-flow-induced shear stress and cyclic mechanical strain have also been shown to impact the physiological properties of the Caco-2 cells within a microenvironment [14, 15, 18, 23–25]. Co-culture of the Caco-2 cells with other cell types impacts the differentiation and function of these tumor cells [20, 26]. However, it is well-recognized that tissue-cultured cells derived from colon tumors fail to recapitulate normal small intestine cell lineages and function [27, 28]. Cancer cell lines harbor other features including accelerated accumulation of genetic mutations, loss of normal physiologic responses, and adaptations to tissue-cultured growth, *e.g.* the ability to grow in the absence of an ECM, that render them imperfect compared to primary tissue cultures [27–30]. Despite these drawbacks, use of cancer cells dominates microdevice development since native intestinal tissue quickly undergoes differentiation and/or apoptosis when cultured on non-biological surfaces [31–33].

Fortuitously, innovations in intestinal stem-cell culture methods have made it possible to use primary, non-transformed cells to create specialized tissues *in vitro* [34, 35]. With these methods, primary animal and human intestinal stem cells can be used to create multi-cellular structures known as enteroids that mimic many of the aspects of the small intestinal epithelium [11, 36]. The potential for intestinal enteroid technology is enormous as evidenced by the burgeoning number of reports and reviews on the topic [36–38]. Nevertheless, the cystic, spherical architecture of enteroids presents severe limitations in many applications. Current culture systems yield an enteroid with an enclosed lumen buried within a thick mass of Matrigel (a hydrogel) [39]. The luminal aspect of the enteroid is thus not easily accessed by drugs, toxins, probiotics, microbiota and other agents. Furthermore, culture of cells embedded within a hydrogel presents additional problems for assay development including the need for compounds to diffuse through the hydrogel to reach the enteroid, which may lead to artifacts during time sensitive assays, and the potential for dosage errors due to adsorption of the compound into the hydrogel. Thus, there is a pressing need for engineered culture systems to address the enteroid limitations by providing an accessible luminal surface for ready assay performance yet preserving the stem and differentiated cells present in the enteroids.

The combination of advances in the culture of primary stem cells and their differentiated progeny with cutting-edge microengineered systems now makes it possible to develop functional human intestinal epithelium on lab-on-chip devices [40, 41]. Critical to this endeavor are identification of a biomimetic material with appropriate ECMs and stiffness to support both stem and differentiated cells and to construct scaffolding of the proper 3D topography for crypts and villi. When this is combined with tightly controlled environments enabled by microscale devices, sustained, biochemical gradients should be capable of directing a polarized cellular architecture. In this manuscript, we describe our work to identify a cross-linked collagen hydrogel that permits stem cell maintenance and

proliferation as well as formation of the differentiated lineages of the small intestine. This hydrogel was then micromolded on a porous substrate in a 3D topography that recapitulated the crypt/villus architecture of the small intestinal epithelium. This human 3D tissue was then subjected to chemical gradients applied to the basal-luminal axis to create stem/proliferative and differentiated cells zones, formation of appropriate differentiated lineages and cell movement along the crypt-villus axis analogous to that seen *in vivo*.

2. Experimental section

2.1. Materials

Matrigel, sodium bicarbonate, rat tail type I collagen, and Transwell inserts were purchased from Corning. N-acetyl cysteine was obtained from MP Bio. Murine EGF was from Peprotech. Primocin was from InvivoGen. Gastrin was from Anaspec. Nicotinamide, A83-01, sodium periodate, poly(ethylene glycol) methyl ether acrylate monomer, and benzyl alcohol were from Sigma Aldrich. Prostaglandin E2 (PGE2) was from Cayman Chemicals. SB202190 was from Selleckchem. Y-27632 was from ApexBio. Sodium butyrate was from Acros Organics. DAPT was from Xcessbio. Accutase was from STEMCELL Technologies. Collagenase (type IV) was from Worthington Biochemicals. Human collagen (type I) was obtained from Advanced Biomatrix. PTFE porous membrane was from Millipore. The biocompatible transfer adhesive was from 3M. Red alkaline phosphatase substrate kit was from Vector Labs. Antibodies and serum were purchased as follows: rabbit α-Muc2, integrin β4, villin, and ZO-1 were from Santa Cruz; mouse α-cytokeratin 20 (KRT20) was from ProteinTech; rabbit α-olfactomedin-4 (Olfm4) was from Cell Signaling; rabbit α-ezrin was from ThermoFisher; donkey serum and donkey anti-rabbit or mouse IgG conjugated with Alexa Fluor 488 were from Jackson Immunoresearch. Reveal Decloaker antigen retrieval solution was from Biocare Medical. All other reagents were from ThermoFisher Scientific.

2.3. Cell culture media

Medium for expanding stem/progenitor cells either as enteroids (embedding in Matrigel) or monolayers (on the surface of neutralized collagen hydrogel), termed expansion medium (EM), was prepared from a mixture of advanced DMEM/F12 medium, L-WRN conditioned medium, and supplemented with GlutaMAX (1×), B27 (1×), HEPES (10 mM), N-acetyl cysteine (1.25 mM), nicotinamide (10 mM), EGF (50 ng/mL), gastrin (10 nM), prostaglandin E2 (10 nM), SB202190 (3 μM), penicillin (100 unit/mL), streptomycin (100 μg/mL), and primocin (100 μg/mL) [42]. L-WRN conditioned medium was prepared from L-WRN cells (ATCC #CRL-3276) following a published protocol [35]. This cell line produces Wnt-3A, R-spondin 3, and noggin. For the first 48 h after cell isolation or passage, Y-27632 ROCK inhibitor (10 μM) was added to the EM to block apoptosis. Stem medium (SM) was identical to EM, but the TGF β-inhibitor A83-01 (500 ng/mL) was added. Differentiation medium (DM) was identical to SM, but lacked L-WRN conditioned medium. The detailed information about reagents and media compositions is listed in Table S1 and S2.

2.3. Isolation of crypts from human small intestinal surgical specimen

A surgical specimen of human small intestine (jejunum) was obtained from gastric bypass surgery at UNC Hospitals with consent of the patient (under the approved protocol UNC IRB #14-2013). Villi and crypts were detached from the specimen by incubation in a chelating buffer for 75 min at 20 °C followed by vigorous shaking in a 15-mL conical tube. The chelating buffer was composed of EDTA (2 mM), dithiothreitol (DTT, 0.5 mM, freshly added), Na_2HPO_4 (5.6 mM), KH_2PO_4 (8.0 mM), NaCl (96.2 mM), KCl (1.6 mM), sucrose (43.4 mM), D-sorbitol (54.9 mM), pH = 7.4 [43]. A few hundred crypts were obtained from the small clinical specimen. Released crypts were placed into either enteroid or monolayer culture systems less than 30 min after isolation.

2.4. Enteroid culture system based on Matrigel encapsulation

Isolated crypts were encapsulated in Matrigel for enteroid culture as described previously [35, 43]. Briefly, 1,000 crypts (admixed with villi) were suspended in 60 μL of cold Matrigel and then a 15 μL suspension was added to each well of a 24-well plate. After gelation of the Matrigel at 37 °C for 15 min, 500 μL of EM was added to each well. The EM was refreshed every 48 h. Every 4–5 days, the enteroids were dissociated with Accutase and passaged to a new 24-well plate at a ratio of 1:3.

2.5. Monolayer culture system on the surface of neutralized collagen hydrogel

Neutralized collagen hydrogel (1 mg/mL, pH 7.4, rat tail) was prepared in 6-well plates for the monolayer culture. Collagen (dissolved in 0.02 N acetic acid) was neutralized with sodium hydroxide (1.15 molar equivalent of acetic acid), HEPES (20 mM), sodium bicarbonate (53 mM), and phosphate-buffered saline (PBS, 1×) at 4 °C with a final pH of 7.4 to generate a 1 mg/mL solution. 1 mL of the solution was added to each well of the 6-well plate and incubated at 37 °C for 1 h to generate a clear hydrogel. PBS was used to cover the hydrogel during storage. Before plating epithelial cells, the collagen hydrogel was rinsed with PBS for 5 min ×3. Enteroids were converted to monolayers by first extracting them from the Matrigel patty by pipetting the gel in buffer using a 200 μL pipet tip, dissociating them with Accutase, and then plated the cells on the top of a collagen hydrogel and cultured in EM. The EM was refreshed every 48 h. When the cell surface coverage was greater than 70% (typically 5–7 days), the monolayers were passaged by a two-step dissociation method. In the first step, the monolayer was detached from the collagen hydrogel by scraping the collagen (with attached cells) from the well, and transferring the gel/cells to a 15-mL conical tube containing 1 mL EM with 500 U/mL of collagenase (Type IV, 500 U/mL). The gel was then fragmented into small pieces by repetitive pipetting. The suspension was then incubated at 37 °C for 10 min to completely digest the collagen gel. The monolayer fragments were pelleted by centrifugation at 600 × g for 1 min, rinsed with 5 mL PBS, and pelleted again. The second step was to break up the monolayer into small fragments by incubating the pellet in 150 μL PBS containing EDTA (0.5 mM) and Y-27632 (10 μM) at 37 °C for 5 min. The monolayers were repetitively pipetted to create smaller fragments. The cell fragments were re-suspended in EM and sub-cultured on a new collagen hydrogel at a passage ratio of 1:3. To ensure that the cells possessed normal chromosomes, cells were karyotyped

(KaryoLogic, Inc) at passage number P3 and P15. Twenty cells from each sample were analyzed. Cells were never used beyond P15.

2.6. Lineage differentiation

Lineage differentiation was performed using a method adapted from that published previously [44]. Cells were cultured as monolayers in EM for 4 days followed by moving the cells to DM to initiate cell differentiation. Sodium butyrate (abbreviated as “B”, 5 mM) or gamma-secretase inhibitor DAPT (abbreviated as “D”, 10 μM) was added as indicated.

2.7. Cross-linking collagen hydrogel by EDC/NHS chemistry

To improve the collagen integrity, collagen was cross-linked with 1-ethyl-3-(3-dimethylaminopropyl)carbodiimide hydrochloride (EDC) and N-hydroxysuccinimide (NHS) at pH 5 [45]. Collagen solution (in 0.02 N acetic acid) was lyophilized for 72 h to remove water and acetic acid. The lyophilized collagen was dissolved in 2-(N-morpholino)ethanesulfonic acid (MES) buffer (0.1 M, pH 5) at a concentration of 5 mg/mL. To prepare cross-linked collagen, 4 mg/mL collagen, 60 mM EDC and 15 mM NHS in MES buffer (0.1 M, pH 5) were mixed in a conical tube on ice. Air bubbles were removed by centrifugation at 3,000 × g for 1 min. 1 mL of the mixture was added to a well of a 6-well plate. After incubating the hydrogel at 22 °C for 60 min, the collagen scaffold was placed in copious deionized water for 24 h to remove excess EDC and NHS. The hydrogel was sterilized with 75% ethanol, rinsed with PBS ×5, and stored in PBS at 4 °C. The Young’s modulus of the cross-linked collagen was 9.5±0.6 KPa (n=3) measured by atomic force microscopy (MFP-3D, Asylum Research) by recording force versus indentation and fitting the curves to the Hertz model [46]. A polystyrene spherical tip (Novascan Technologies) with a radius of 2.25 μm and a spring constant of 31.9 pN/nm was used for these measurements. Prior to plating cells on the cross-linked collagen, the collagen was incubated overnight in 4 mL PBS containing 10 μg/mL human collagen at 37 °C.

2.8. Fabrication of collagen microwell scaffold on a modified Transwell insert

2.8.1. Microfabrication and surface modification of polydimethylsiloxane (PDMS) stamps—1002F photoresist was used to prepare a master mold for the PDMS stamps. 1002F was comprised of 1002F resin, photoinitiator (triarylsulfonium hexafluoroantimonate salts), and solvent (gamma-butyrolactone) as previously described [47]. The weight ratio of resin:photoinitiator:solvent was 65:6.5:28.5. A 500-μm thick film of 1002F was produced by spin-coating 1002F photoresist on a glass slide (75 mm × 50 mm × 1 mm). The film was baked at 95 °C for 60 min to evaporate the solvent, and was then exposed to UV light (1500 mJ/cm^2) through an initial photomask with an array of 170-μm dark circles. A post-exposure baking step was next performed in a 95 °C oven for 10 min followed by baking on a 120 °C hotplate for 10 min. A second layer of 132-μm thick 1002 photoresist was spin-coated onto the surface of the first resist layer. The film was exposed to UV light (1000 mJ/cm^2) through a second photomask with an array of open circles 60 μm in diameter. The film was post-exposure baked as above and then developed with propylene glycol monomethyl ether acetate (PGMEA). The film was baked on a 120 °C hotplate for 60 min to harden the film.

PDMS stamp #1 was created from the above 1002F master mold by spreading PDMS pre-polymer on the mold followed by de-gassing under a vacuum. PDMS on the mold was baked in a 95 °C oven for 30 min followed by demolding. PDMS stamp #1 contained an array of rounded-top posts for the villi alongside flat-bottomed microwells for the crypts. PDMS stamp #1 was treated with a plasma for 2 min, and coated with octyltrichlorosilane using a vapor-phase process for 16 h. A second PDMS stamp (stamp #2) was replicated in the same manner from stamp #1 to create a negative replica.

PDMS stamp #2 was trimmed to a size of 6 mm × 6 mm, and coated with poly(ethylene glycol) to eliminate collagen adhesion during molding. The PDMS stamps were surface-grafted with poly(ethylene glycol) as described previously using UV-mediated graft polymerization [48]. Briefly, the PDMS stamps were placed in a glass tube with a screw-cap. The tube was filled with a mixture of 10 wt% poly(ethylene glycol) methyl ether acrylate monomer, 0.5 mM sodium periodate, 0.5 wt% benzyl alcohol in water. The tube was then exposed to UV radiation in a Loctite 7411-S UV Flood System for 4 h. The stamps were then rinsed with deionized water and soaked in deionized water overnight to remove non-covalently bound polymer and monomer. The grafted stamps were stored in 75% ethanol until use.

2.8.2. Micromolding/cross-linking collagen scaffolds on a modified Transwell insert—A collagen scaffold was micromolded and cross-linked on the surface of a porous PTFE membrane (0.4 μm pore size) held in a 12-well insert. To construct the insert, the polycarbonate porous membrane was removed from a commercially available Transwell insert and a hydrophilic PTFE porous membrane was attached to the insert using a biocompatible transfer adhesive. To reduce the effective area of the porous membrane from 12-mm to 3-mm in diameter, the backside of the membrane was partially sealed off by attaching a non-permeable COC plastic film of 200 μm thickness. This reduced the effective area of the porous membrane to 7.1 mm^2. Next a mixture of 4 mg/mL collagen, 60 mM EDC and 15 mM NHS in MES buffer (0.1 M, pH 5) was prepared, and bubbles were removed by centrifugation at 3,000 × g for 1 min. The collagen mixture (50 μL) was added to the center of the modified insert, and PDMS stamp #2 was placed on the top of the mixture. To remove the trapped air bubbles amongst the microposts or inside microwells of the stamp, the 12-well plate was pressurized under 40 psi nitrogen for 2 h. The PDMS stamp was then removed from the collagen scaffold. The collagen scaffold was soaked in 2 liters of deionized water for 24 h with multiple water exchanges to remove unincorporated EDC and NHS [45, 49, 50]. Scaffolds were sterilized in 75% ethanol for 5 min, rinsed with PBS for 5 min × 3, and stored in PBS at 4 °C until use. The total thickness of the collagen layer was ~669 μm (477 μm-tall villi, 132 μm-deep crypts with a 60 μm-thick gel layer beneath the crypt well).

2.9. Generating crypt-villus architecture of human small intestinal epithelium by culturing cells on the collagen scaffold followed by imposition of a biochemical gradient—The modified Transwell insert enabled a diffusion-based gradient to be established across the collagen hydrogel and membrane when the upper and lower reservoirs were loaded with different media *e.g.* SM and DM media. The upper and lower

reservoirs were sufficiently large that they acted as an infinite sink and source over 24 h when the media was replaced every 24 h. To confirm that the lower (SM) and upper (DM) reservoirs acted as an infinite source and sink, PBS with fluorescein-dextran (100 μg/mL, MW=40,000, which is close to MW of Wnt-3A proteins) was added into the bottom or SM reservoir of the Transwell (with micromolded scaffold, but no cells). PBS alone was added into the top or DM reservoir. After 24 h, the concentration of fluorescein-dextran in the top or DM compartment was 4.0±1.0 μg/mL, and that in the bottom or SM reservoir was 98.2±1.0 μg/mL (n=3). Thus, over the course of 24 h, the concentration of the reagents in the lower and upper reservoirs could be approximated as constant so that a stable, diffusion-based gradient was formed across the collagen scaffold.

Just prior to use, the micromolded collagen scaffold was incubated overnight with 10 μg/mL human collagen in PBS at 37 °C. Cell fragments obtained from one well of neutralized collagen hydrogel in a 6-well plate were dispersed on four separate scaffolds housed within the modified Transwell inserts. The cells on the scaffold were cultured in 3 mL EM per insert (1 mL in the upper compartment, and 2 mL in the bottom compartment). The medium was exchanged every two days. Once the cells covered the entire surface of the scaffolds, typically 7 days, a gradient of growth factors was applied across the shaped collagen scaffold. DM (0.5 mL) was placed in the top compartment, and SM (1.5 mL) was loaded into the bottom compartment. The DM and SM were replenished daily.

2.10. EdU/ALP/Muc2/nuclei four-color staining protocol

Cell proliferation and differentiation were assessed with a four-color fluorescence staining protocol. Cells were incubated with 5-ethynyl-2-deoxyuridine (EdU, 10 μM) in medium for 24 h at 37 °C. The living cells were washed in PBS and incubated for 30 min at 37 °C with alkaline phosphatase (ALP) substrate in Tris buffer (0.15 M, pH 8.4), rinsed with PBS, fixed in 4% paraformaldehyde for 15 min and then permeabilized with 0.5% Triton X-100 in PBS for 20 min. The proliferative cells were stained with a Click-iT EdU Alexa Fluor 647 imaging kit. Subsequently, the cells were rinsed with 0.75% glycine in PBS for 5 min ×3, followed by blocking with 10% donkey serum for 1 h at 20 °C. Cells were then incubated in rabbit α-Muc2 (1:200) at 4 °C for overnight, and stained with donkey anti-rabbit IgG conjugated Alexa Fluor 488 (1:500) for 45 min at 20 °C. Nuclei were stained with Hoechst 33342 (2 μg/mL) for 15 min at 20 °C.

2.11. Cryosection and immunofluorescence

Specimens were fixed in 4% paraformaldehyde for 15 min, rinsed with PBS, and incubated overnight in 30% sucrose at 4 °C. The tissue was then embedded in a cryo-embedding medium (OCT). The frozen tissue block was sectioned into 10-μm thick films with a cryostat. Primary antibodies used were against olfactomedin-4 (Olfm4) (1:500), cytokeratin 20 (KRT20) (1:500), Muc2 (1:200), ezrin (1:200), villin (1:200), integrin β4 (1:200), and ZO-1 (1:200). Antigen retrieval was performed on specimens stained for Oflm4 and KRT20 by incubating the sample in a antigen-retrieval solution at 95 °C for 15 min and then allowed to cool for 15 min. The sections were rinsed with PBS, and blocked with 10% donkey serum for 1 h at 20 °C. All sections were incubated with the primary antibody overnight at 4 °C followed by incubation with secondary antibody, donkey anti-rabbit or mouse IgG

conjugated with Alexa Fluor 488 or 594 (1:500). Nuclei were stained with Hoechst 33342 (2 μg/mL) for 15 min. Alexa Fluor 488 phalloidin was used to stain filamentous actin (F-actin).

2.12. Image acquisition, analysis, and statistics

Specimens were imaged using a Nikon Eclipse TE300 inverted epifluorescence microscope equipped with DAPI/FITC/Texas Red/CY5 filter sets. Images were acquired at randomly selected locations with a 10× objective (N.A. = 0.3). S-phase cells stained with the Click-iT EdU stain were imaged using a CY5 filter (excitation filter 604–644 nm, emission 672–712 nm), ALP stain was imaged employing a Texas Red filter (excitation filter 542–582 nm, emission 604–644 nm), Muc2 immunofluorescence was visualized with a fluorescein filter (excitation filter 450–490 nm, emission 520 nm long pass), and nuclei stained with Hoechst 33342 was identified using a DAPI filter (excitation filter 352–402 nm, emission 417–477 nm). Images were empirically thresholded using Image J (https://imagej.nih.gov/ij/). ImageJ was also used to measure the percent surface area of each image displaying supra-threshold fluorescence from the EdU, ALP or Muc2 stains. These areas were then normalized to the total cell area by dividing by the area of the Hoechst fluorescence (nuclei stain). Four randomly selected locations in the same monolayer were used to generate the image data and this experiment was repeated (n = 4). The average with a single standard deviation is shown unless otherwise specified. Statistical analysis was performed using a one-way analysis of variance (ANOVA) followed by a multiple comparison test with Tukey's honestly significant difference procedure conducted at the 5% significance level. Multiple comparison testing was performed on all experimental groups. ANOVA analyses and subsequent multiple comparisons were performed using MATLAB (MATLAB 2014b, The MathWorks, Inc., Natick, Massachusetts). In all figures, '*' denotes $p < 0.05$ and '**' $p < 0.005$.

To assess the polarity of the *in vitro* villus/crypt, the side view of the crypt/villus samples was obtained by scraping the tissue off the scaffold with a tungsten dissecting needle. Horizontally positioned crypts/villi were then imaged using standard fluorescence microscopy.

3. Results

3.1. Human small intestinal epithelium loses the crypt/villus architecture in the enteroid culture system

In vivo, human small intestinal epithelium demonstrates three prominent attributes: distinctive shaped crypts and villi, compartmentalization of cell types, and a luminal surface contacting the intestinal contents (Fig. 1A and B). The epithelium is comprised of an array of projections (villi) with interspersed invaginations (crypts). The villi are covered primarily with non-dividing differentiated ($KRT20^+$) cells, while the majority of cells within the crypts are proliferative ($Olfm4^+$) [51, 52]. The bases of the crypts host the stem cells within a supportive microenvironment or niche to maintain the stem cells in their undifferentiated state as well as to enable their proliferation to generate progenitors or transit amplifying cells to replenish the short-lived, differentiated cells. The terminally differentiated cells are preferentially located on the villi physically segregated from the stem/proliferative cells.

When pre-isolated stem cells or crypts (with their stem cells) were cultured within a Matrigel patty, cell segregation was rapidly lost (Fig. 1A, C and D) [39]. The stem cells proliferated to form cystic structures, termed enteroids, possessing an enclosed lumen bordered by a single layer of epithelial cells (Fig. 1C). The enteroids were non-polarized and comprised predominantly of proliferative cells (EdU^+, $Olfm4^+$) with few differentiated cells ($KRT20^+$) present (Fig. 1D). The proliferative cells were randomly intermixed with the few non-dividing, differentiated cells present. While the enteroid culture system has transformed the study of the small intestine, these enteroids bear little resemblance to the *in vivo* tissue and are unsuitable for study of many small intestine functions, such as stem cell compartment dynamics, cell migration and differentiation, chemical gradient influence, and microbiome interactions.

3.2. A cross-linked collagen hydrogel supports growth of human small intestinal cells as a proliferative monolayer undergoing differentiation in response to biochemical cues

We developed a cross-linked collagen hydrogel as a matrix to support the growth of human small intestinal cells as monolayers. Both carboxylic acid and primary amine groups are abundant in collagen [53]. In the presence of EDC and NHS, the carboxylic acid group of one chain of collagen is converted to a reactive NHS ester that subsequently reacts with a primary amine goup of the other chain of collagen to form a stable amide bond to covalently cross-link the collagen. During reaction, EDC/NHS acts to catalyze cross-linking and are not incorporated into the collagen, thus the EDC/NHS can be removed from the collagen gel after the reaction avoiding any negative impact on subsequent cell culture. The cross-linked collagen hydrogel possessed a modulus of 9.46±0.64 KPa (n=3). The cross-linked collagen possessed sufficient stiffness that the traction forces exerted by cells did not deform the collagen. To compensate for the possible loss of ECM contacts caused by cross-linking as well as the rat source of the collagen, the hydrogel was coated with a thin layer of human collagen prior to cell plating. Human small intestine fragments were cultured on the collagen surface in the presence of expansion medium (EM) for 4 days followed by stem medium (SM) for 4 days, which contained Wnt-3a, R-spondin 3, noggin and was optimized to support the proliferation of stem cells by activating Wnt signaling (Fig. 2A). The cells grew as a monolayer comprised predominantly of EdU^+ proliferative cells with very few differentiated cells present as indicated by low or absent alkaline phosphatase (ALP) activity (or absorptive enterocytes) and mucin 2 (Muc2) immunostaining (or goblet cells) (Fig. 2B and C). The presence of cell consistent with stem cells ($Olfm4^+$) were observed in the monolayer (Fig. 2D). The EDU^+ and $Olfm4^+$ cells (stem/proliferative cells) were distributed randomly throughout the monolayer so that a stem or proliferative cell compartment was not observed.

Since differentiated and stem cells co-exist in the epithelium of the native intestine, scaffolding for culture of small intestinal cells should support formation of differentiated cells in addition to stem cells. To determine whether the stem/proliferative cells grown as monolayers could be differentiated in a similar manner as those grown as enteroids [44], the monolayers were cultured in differentiation medium (DM) without growth factors. Differentiated cell markers (Muc2, ALP) increased indicating increased numbers of absorptive enterocytes and goblet cells. In contrast proliferation (EdU incorporation)

decreased relative to that of the control monolayers in SM suggesting a decline in the numbers of stem/proliferative cells under these conditions (Fig. 2B and C). *In vivo* cells of the small intestine are highly polarized with the luminal membrane surface and cytoplasm displaying proteins that participate in transport/absorption or its supporting infrastructure such as actin and ezrin which are at high concentration within the microvilli [54]. In contrast, other molecules such as integrin-β4 are localized to the basal membrane region providing interactions with the ECM underling the cells [55]. The differentiated monolayers on the collagen surface exhibited an appropriate basal-luminal polarity with actin and ezrin concentrated at the luminal surface (microvilli) and integrin-β4 at the basal surface. Mucin-2, a component of the intestinal mucous layer, lines the luminal surface protecting cells from digestive products and microbes [56]. In the monolayers, Muc2 was present only at the luminal cell surface indicating that mucous was secreted in the luminal direction only (Fig. 2D). Tight interconnections between cells formed by tight and adherens junctions block leakage of bile, microbes and other harmful entities into the underlying tissue [57]. The monolayers on collagen displayed properly localized β-catenin in the basolateral cell region and ZO-1 indicating the presence of adherens and tight junctions. These data demonstrate that monolayers were responsive to external cues in a manner similar to enteroids. More importantly, the proliferative monolayers differentiate into a fully polarized epithelial cell with key features of *in vivo* small intestinal cells.

Modulation of notch signaling is reported to alter proliferation and differentiation of intestinal epithelial stem cells in enteroids [58]. Gradients of a notch signaling activator and inhibitor were applied to the monolayer to determine whether the monolayers responded in a manner similar to that of enteroids. Gamma secretase inhibitors (GSI) diminish Notch signaling by blocking proteolytic activation of Notch receptors leading to differentiation of proliferative cells into goblet cells [59, 60]. For this reason, GSI (10 μM DAPT) was added to DM for culture of the monolayer. An increase in goblet cells ($Muc2^+$) was not observed as in the enteroids, but formation of absorptive enterocytes (ALP^+) was greatly increased relative to that of DM alone (Fig. 2B and C). Butyrate or short chain fatty acids are reported to act as Notch1 activator [61]. Addition of butyrate (5 mM) to DM did not significantly increase ALP or Muc2 expression relative to DM only. Butyrate also initiated rapid cell death in the small intestine epithelial cells probably due to its effect as a histone deacetylase (HDAC) inhibitor [62]. This effects of DAPT and a short chain fatty acid on the monolayers is different from that reported for enteroids [44], potentially due to addition of the molecules directly to the luminal surface of the monolayer rather than to the basal surface as occurs in the enteroid system.

3.3. The cross-linked collagen scaffold can be micromolded in the anatomical shape of the human small intestinal epithelium

PDMS stamps possessing the true (stamp #1) and reversed (stamp #2) architecture of the human small intestinal epithelium were fabricated through multiple steps including two-layer photolithography and soft lithography replica molding (Fig. 3A). Microwells representing the negative of the villi were first patterned into an epoxy photoresist using standard spincoating and photo-illumination steps. In a similar fashion, a second layer of photoresist was patterned with micropillars or negatives of the crypts. To create the rounded

surfaces of the villi, a shortened rinse/development cycle was used for the photoresist master mold to leave a small amount of the resist at the bottom of the villi microwells. During the hard bake used to form the mold, the photoresist residue melted, reflowed and formed a meniscus inside the microwell creating a curved surface. The geometry of the microstructures (stamp #1) shown in Fig. 3B was designed to simulate the anatomical shape of the *in vivo* human duodenal epithelium (villus height = 437±98 μm, villus width = 149±41 μm, crypt depth = 193±37 μm, mucosal thickness = 642±128 μm, and crypt to villus ratio= 2.26±0.57, n=10 [63]). On PDMS stamp (#1), the villus height = 477 μm, villus width = 170 μm, crypt depth = 132 μm, crypt width = 60 μm, total height of crypt/villus = 609 μm, and crypt to villus ratio = 2. After formation of the master mold in photoresist, two sequential rounds of soft lithography were used to form a PDMS replica of the master mold. The microscopic images of the PDMS stamps (#1) show six wells (for crypts) surrounding a single pillar (for villus) (Fig. 3C and D). The surface of PDMS stamps (#2) was covalently grafted with polyethylene glycol to eliminate collagen adhesion during molding.

To reproduce the surface topography of the small intestinal epithelium, PDMS stamp #2 was pressed into the surface of collagen overlaid onto the porous membrane in a modified Transwell insert (Fig. 3E). An array of rounded pillars (villi) and adjacent microwells (crypts) formed from in the cross-linked collagen as it gelled. Each villus/crypt array possessed approximately 90 pillars or villi structures and 180 microwells or crypt structures in the region above the porous membrane in contact with the basal reservoir below the modified insert (Fig. 3F). When viewed by brightfield microscopy, the villi were readily visualized as protruding above the surface while the much smaller crypts dipped below the plane of the epithelial surface (Fig. 3G). The shaped scaffolding in the modified insert was placed into a standard 12-well plate to create separate upper (luminal) and lower (basal) fluid reservoirs enabling distinct solutions to be applied to the upper and lower surfaces of the molded collagen.

3.4. Human small intestinal cells form a monolayer covering the shaped collagen scaffold

Cells were plated on the scaffolds and cultured under expansion medium (EM) in both the luminal and basal reservoirs (Fig. 4A). The crypt/villus surfaces were covered in a monolayer of cells within 9 days (Fig. 4B). On a randomly selected location (2.246 × 1.677 mm), 79% of 108 crypts were observed to be lined with cells, and 100% of 56 villi were completely covered with cells. Ten arrays were fabricated all were successfully covered with a cell monolayer. As the cells grew to cover the scaffold surface, the cells were easily visualized as high-contrast darker regions rimming the inside of the crypts or outside of the villi (Fig. 4B). No multilayered cell regions were observed (see also Fig. 5 and 6). Adjusting the microscopy focal plane either upward or downward enabled visualization of cells within the crypt lumen or on the villus top surface (Fig. 4C and D). Crypts lined with cells possessed visible lumens (Fig. 4C). When pulsed with EdU, proliferative cells occupied the crypt walls as well as the majority of the villi surface. The EdU^+ cells were randomly distributed across the array surface and suggested that the entire array crypt plus villus surfaces were covered with stem/proliferative cells. The created *in vitro* tissue possessed a crypt-villus architecture but without proper stem and differentiated cell segregation in the crypts and villi (Fig. 4D).

3.5. Application of chemical gradients across the cell-covered scaffold creates stem/proliferative and differentiated cell compartments

Human small intestinal cells were cultured on a scaffold until a confluent crypt-villus array was formed by visual inspection (typically 7 days). To polarize the *in vitro* crypt-villus architecture, a gradient of 3 growth factors (Wnt-3A, R-spondin 3 and noggin) was applied along the crypt-villus axis by placing DM in the luminal or upper fluid reservoir and SM in the basal or lower reservoir. Selection of the 3 factors for the gradient was based on prior work demonstrating that Wnt-3A and R-spondin activate the Wnt signaling pathway to support stem cells while Noggin inhibits BMP to block differentiation [44, 51, 52, 64]. Thus Wnt-3A, R-spondin and Noggin are all critical for stem cell maintenance but not for formation of the differentiated lineages particularly enterocytes. The DM and SM were replaced every 24 h so that the reservoirs acted as an infinite source and sink maintaining a linear gradient of 3 growth factors across the collagen scaffolding (Fig. 5A). After culture for 4 days under the gradient, a polarized tissue with proliferative cells (EdU^+) confined to the crypts and adjacent regions, but absent from the villi, was formed (Fig. 5B and C). Thus a simple linear gradient of three factors was sufficient to create a proliferative (crypt) and non-proliferative (villus) compartment in the small intestinal construct (Fig. 5D). On the array possessing 90 cell-covered-villi and 127 cell-lined-crypts shown in Fig. 5D, 100% of villi possessed no EdU^+ cells on their uppermost region while 96% of crypts were lined with EdU^+ cells. These data suggested that a stem cell compartment might exist within the crypts. To determine whether the villi hosted differentiated cells as they do *in vivo*, the construct developed under the growth-factor gradient was stained for alkaline phosphatase (ALP) activity. Very few ALP^+ cells were observed on the tissue indicating that the non-proliferating villus cells were unable to differentiate under these conditions (Fig. 5B and C). Thus, a true differentiated cell compartment was not created by this 3-factor gradient. To generate a crypt-villus tissue with compartmentalized stem and differentiated cells, DAPT in DM was added to the luminal side while SM was placed in the basal reservoir (Fig. 5E). This bidirectional gradient localized the proliferative cells to crypts as before, but also induced the formation of absorptive enterocytes (ALP^+) on the villi (Fig. 5F and G). ALP^+ cells were not observed within the crypts. To define the location of the stem/proliferative cells, the constructs were sectioned and stained for Olfm4, a marker for stem and proliferative cells. $Olfm4^+$ cells were confined to the crypts and adjacent regions (Fig. 5H) recapitulating the Olfm4 staining profile of primary tissue (Fig. 1B). KRT20 (human cytokeratin 20) marks terminally differentiated tissues of the intestine (Fig. 1B) and was localized to the villi tips in the *in vitro* small intestinal epithelium (Fig. 5H). KRT20 immunostaining was absent from the crypts and adjacent regions. With respect to cell compartmentalization and architecture, the *in vitro* epithelium with crypts and villi displayed a marked resemblance in shape, polarity and luminal accessibility to that of *in vivo* tissue shown in Fig. 1B.

3.6. Proliferative cells in the crypts migrate upward into the villi over time

Directional migration of cells along the crypt/villus axis is an important *in vivo* renewal property of the intestinal epithelium. To maintain a homeostatic epithelial barrier, stem and progenitor cells proliferate and their offspring migrate up the villi to replenish the short lived differentiated cells that shed into the intestinal lumen [65]. To assess whether the *in vitro*

tissue construct recapitulated this *in vivo* movement of cells, the polarized tissue (4 days under gradient of growth factors) was labeled with EdU for 24 h. EdU was removed and the cells on the scaffold cultured for an additional 96 h under the gradient. At 0 h after EdU washout, the majority of EDU^+ cells resided within the crypts and adjacent regions and EdU^+ cells did not appear on the villi (Fig. 6A). At 96 h after removal of the EdU, EdU^+ cells were readily observed along the length of the villi demonstrating that the EdU^+ cells were migrating up the crypts and onto the villi (Fig. 6B). The migration of proliferative cells up the crypt-villus axis was quantified by measuring the distance that EdU^+ cells moved during the 96 h after the EdU pulse (Fig. 6C). The cell migration rate was on average 40 μm/day, which lies in the range of cell migration rates observed in animal experiments, *e.g.* 38–63 μm/day for neonatal rat small intestine [66].

4. Discussion

Expansion of primary intestinal stem cells *in vitro* requires an appropriate biochemical and biophysical environment. Biochemically, a cocktail of soluble growth factors (mainly Wnt-3A, R-spondin and noggin) and small molecules are required to modulate cell signaling (Wnt, BMP) to promote stem cell maintenance and proliferation. A suitable matrix with proper ECM proteins and biophysical properties is required to act as a scaffolding for physical support of the cells. The enteroid culture system fulfills both requirements enabling expansion of human small intestinal stem cells *in vitro* [35]; however, the system yields 3D enteroids rather than the exposed 2D monolayer covering the intestinal surface probably due to the extremely low stiffness of the Matrigel (Young's modulus = 50 Pa [67]).

To recapitulate the topography and cell behavior of the small intestinal epithelium as an organ-on-chip, a material other than Matrigel is needed to provide a suitably shaped scaffolding material. The material must: (1) have proper biophysical properties (stiffness, ECM contacts) to support monolayer formation with both stem and differentiated cells; (2) be sufficiently porous to allow diffusion of molecules through the matrix; (3) be compatible with a microfabrication process to generate microstructures; (4) maintain its integrity during long term culture of cells. Plastics and rubbers (*e.g.* polystyrene and PDMS) are impermeable to soluble molecules and possess high stiffness (Young's modulus of polystyrene =3–3.5 GPa [68], PDMS = 0.8–4 MPa [69]). PDMS has been microfabricated into stretchable porous membranes for building a Caco-2 cell-based human gut-on-a-chip [15], but this device did not support long-term culture of primary human small intestinal cells [70]. A porous biodegradable poly(lactic-co-glycolic acid) (PLGA, stiffness = 1–2 GPa [71]) has been micromolded into high-aspect ratio pillars to allow growth and differentiation of enteroids [72], but support of stem cells was not demonstrated. Polystyrene and PDMS while coomon materials in fabrication of microdevices, do not possess the properties required for the self-renewal of intestinal stem cells.

Neutralized collagen hydrogel possesses a stiffness of 100–1,000 Pa (depending on collagen type and concentration) and has been identified to support both enteroid [73] and monolayer [74] formation of primary intestinal epithelial stem cells. The neutralized collagen hydrogel also supported the self-renewal of human small intestinal stem cells in 2D monolayers in this report. It is likely that the collagen hydrogel closely mimics the *in vivo* intestine's basement

membrane in terms of porosity, ECM proteins and stiffness. While the collagen hydrogel supported human small intestinal stem cells as monolayers, this hydrogel is unsuitable for building 3D microstructured scaffolds due to its low strength. We attempted to micromold and shape a collagen hydrogel into high-aspect ratio microwells, but found that growth of the primary intestinal cells on the surface rapidly destroyed the scaffold eliminating the microstructures. This was likely due to the inability of the native collagen to resist the traction forces applied by cells on the matrix as well as collagen's susceptibility to protease remodeling mediated by the cells [75]. The low strength of collagen hydrogel was addressed by chemically cross-linking the collagen. Collagen hydrogels, micromolded into high aspect ratio micropillars and then cross-linked with glutaraldehyde, supported the proliferation of Caco-2 cells without cell induced deformation [76]. Here we used a different method to cross-link collagen. An acidic solution of collagen was mixed with EDC and NHS to allow the cross-linking reaction to occur prior to fiber aggregation. The resulting collagen hydrogel is optically clear, possessing a stiffness of 9,460 Pa. Human small intestinal cells proliferated on the cross-linked collagen hydrogel and underwent forced differentiation when placed in the appropriate chemical environment. In addition, the cross-linked collagen was readily molded into microwells and micropillars to mimic the anatomical shape of the human small intestinal epithelium. Cell induced deformation of the scaffolding was not observed. The cross-linked collagen hydrogel is also porous enabling the establishment of a gradient across the scaffold to polarize the stem cells populated on its surface. Thus, the cross-linked collagen hydrogel act as an excellent scaffold for construction of an *in vitro* replica of the small intestinal epithelium from primary cells.

5. Conclusions

A cross-linked collagen hydrogel was identified as a suitable biomimetic scaffold to support *in vitro* culture of primary human small intestinal epithelial cells both as proliferative and differentiated cells, with differentiated cell formation responsive to external biochemical cues. The cross-linked collagen hydrogel was molded into micropillars and microwells to replicate the anatomical shape of the human small intestinal epithelium. Cells plated on the scaffolds were guided to form a crypt-villus architecture, which was then polarized by application of gradients of soluble biochemical reagents along the crypt-villus axis. The *in vitro* human small intestinal tissue mimicked the *in vivo* tissue in terms of architecture, tissue polarity and luminal accessibility. We expect this platform will serve as a physiologically relevant experimental mimic for studying the effect of nutrients, prebiotics, medicines, microbiota, and toxins on human small intestinal epithelium. The platform should find significant utility in translational studies, for example, in high-content screening of pharmaceuticals and microbiota therapeutics since the platform utilizes normal human tissue rather than mouse primary cells or human tumor cells. Finally, the use of human biopsy material enables construction of disease-specific mimics for the better understanding of human pathophysiology as well as disease amelioration.

Supplementary Material

Refer to Web version on PubMed Central for supplementary material.

Acknowledgments

Research reported in this publication was supported by the National Institutes of Health under award number R01DK109559 to N.L.A., S.B., and S.M. The authors thank Bailey Altizer for coordinating the procurement of human small intestine.

References

1. Volk N, Lacy B. Anatomy and Physiology of the Small Bowel. Gastrointest Endosc Clin N Am. 2017; 27:1–13. [PubMed: 27908510]
2. Wang L, Murthy SK, Fowle WH, Barabino GA, Carrier RL. Influence of micro-well biomimetic topography on intestinal epithelial Caco-2 cell phenotype. Biomaterials. 2009; 30:6825–34. [PubMed: 19766306]
3. Hall, JE. Textbook of Medical Physiology. 13. Physiology, G., editor. Philadelphia: W.B. Saunders; 2015.
4. Pageot LP, Perreault N, Basora N, Francoeur C, Magny P, Beaulieu JF. Human cell models to study small intestinal functions: recapitulation of the crypt-villus axis. Microsc Res Tech. 2000; 49:394–406. [PubMed: 10820523]
5. Sommer F, Backhed F. Know your neighbor: Microbiota and host epithelial cells interact locally to control intestinal function and physiology. Bioessays. 2016; 38:455–64. [PubMed: 26990415]
6. von Martels JZ, Sadaghian Sadabad M, Bourgonje AR, Blokzijl T, Dijkstra G, Faber KN, et al. The role of gut microbiota in health and disease: In vitro modeling of host-microbe interactions at the aerobe-anaerobe interphase of the human gut. Anaerobe. 2017
7. Kaiko GE, Ryu SH, Koues OI, Collins PL, Solnica-Krezel L, Pearce EJ, et al. The Colonic Crypt Protects Stem Cells from Microbiota-Derived Metabolites. Cell. 2016; 165:1708–20. [PubMed: 27264604]
8. Lynch SV, Pedersen O. The Human Intestinal Microbiome in Health and Disease. New England Journal of Medicine. 2016; 375:2369–79. [PubMed: 27974040]
9. Yeung TM, Chia LA, Kosinski CM, Kuo CJ. Regulation of self-renewal and differentiation by the intestinal stem cell niche. Cell Mol Life Sci. 2011; 68:2513–23. [PubMed: 21509540]
10. Yu J, Carrier RL, March JC, Griffith LG. Three dimensional human small intestine models for ADME-Tox studies. Drug Discov Today. 2014; 19:1587–94. [PubMed: 24853950]
11. Stelzner M, Helmrath M, Dunn JCY, Henning SJ, Houchen CW, Kuo C, et al. A nomenclature for intestinal in vitro cultures. American Journal of Physiology-Gastrointestinal and Liver Physiology. 2012; 302:G1359–G63. [PubMed: 22461030]
12. Chen Y, Lin Y, Davis KM, Wang Q, Rnjak-Kovacina J, Li C, et al. Robust bioengineered 3D functional human intestinal epithelium. Sci Rep. 2015; 5:13708. [PubMed: 26374193]
13. Chi M, Yi B, Oh S, Park DJ, Sung JH, Park S. A microfluidic cell culture device (muFCCD) to culture epithelial cells with physiological and morphological properties that mimic those of the human intestine. Biomed Microdevices. 2015; 17:9966. [PubMed: 26002774]
14. Kim HJ, Huh D, Hamilton G, Ingber DE. Human gut-on-a-chip inhabited by microbial flora that experiences intestinal peristalsis-like motions and flow. Lab Chip. 2012; 12:2165–74. [PubMed: 22434367]
15. Kim HJ, Ingber DE. Gut-on-a-Chip microenvironment induces human intestinal cells to undergo villus differentiation. Integr Biol (Camb). 2013; 5:1130–40. [PubMed: 23817533]
16. Kim SH, Chi M, Yi B, Kim SH, Oh S, Kim Y, et al. Three-dimensional intestinal villi epithelium enhances protection of human intestinal cells from bacterial infection by inducing mucin expression. Integr Biol (Camb). 2014; 6:1122–31. [PubMed: 25200891]
17. Kim SH, Lee JW, Choi I, Kim YC, Lee JB, Sung JH. A microfluidic device with 3-d hydrogel villi scaffold to simulate intestinal absorption. J Nanosci Nanotechnol. 2013; 13:7220–8. [PubMed: 24245233]
18. Kimura H, Ikeda T, Nakayama H, Sakai Y, Fujii T. An on-chip small intestine-liver model for pharmacokinetic studies. J Lab Autom. 2015; 20:265–73. [PubMed: 25385717]

19. Koppes AN, Kamath M, Pfluger CA, Burkey DD, Dokmeci M, Wang L, et al. Complex, multi-scale small intestinal topography replicated in cellular growth substrates fabricated via chemical vapor deposition of Parylene C. Biofabrication. 2016; 8:035011. [PubMed: 27550930]
20. Pusch J, Votteler M, Gohler S, Engl J, Hampel M, Walles H, et al. The physiological performance of a three-dimensional model that mimics the microenvironment of the small intestine. Biomaterials. 2011; 32:7469–78. [PubMed: 21764120]
21. Wang L, Murthy SK, Barabino GA, Carrier RL. Synergic effects of crypt-like topography and ECM proteins on intestinal cell behavior in collagen based membranes. Biomaterials. 2010; 31:7586–98. [PubMed: 20643478]
22. Yu J, Peng S, Luo D, March JC. In vitro 3D human small intestinal villous model for drug permeability determination. Biotechnol Bioeng. 2012; 109:2173–8. [PubMed: 22488418]
23. Esch MB, Sung JH, Yang J, Yu C, Yu J, March JC, et al. On chip porous polymer membranes for integration of gastrointestinal tract epithelium with microfluidic 'body-on-a-chip' devices. Biomed Microdevices. 2012; 14:895–906. [PubMed: 22847474]
24. Kimura H, Yamamoto T, Sakai H, Sakai Y, Fujii T. An integrated microfluidic system for long-term perfusion culture and on-line monitoring of intestinal tissue models. Lab Chip. 2008; 8:741–6. [PubMed: 18432344]
25. Mahler GJ, Esch MB, Glahn RP, Shuler ML. Characterization of a gastrointestinal tract microscale cell culture analog used to predict drug toxicity. Biotechnol Bioeng. 2009; 104:193–205. [PubMed: 19418562]
26. Ramadan Q, Jafarpoorchekab H, Huang C, Silacci P, Carrara S, Koklu G, et al. NutriChip: nutrition analysis meets microfluidics. Lab Chip. 2013; 13:196–203. [PubMed: 23184124]
27. Artursson P, Palm K, Luthman K. Caco-2 monolayers in experimental and theoretical predictions of drug transport. Adv Drug Deliv Rev. 2001; 46:27–43. [PubMed: 11259831]
28. Larregieu CA, Benet LZ. Drug discovery and regulatory considerations for improving in silico and in vitro predictions that use Caco-2 as a surrogate for human intestinal permeability measurements. AAPS J. 2013; 15:483–97. [PubMed: 23344793]
29. Hidalgo IJ, Raub TJ, Borchardt RT. Characterization of the human colon carcinoma cell line (Caco-2) as a model system for intestinal epithelial permeability. Gastroenterology. 1989; 96:736–49. [PubMed: 2914637]
30. Sun D, Lennernas H, Welage LS, Barnett JL, Landowski CP, Foster D, et al. Comparison of human duodenum and Caco-2 gene expression profiles for 12,000 gene sequences tags and correlation with permeability of 26 drugs. Pharm Res. 2002; 19:1400–16. [PubMed: 12425456]
31. Maschmeyer I, Hasenberg T, Jaenicke A, Lindner M, Lorenz AK, Zech J, et al. Chip-based human liver-intestine and liver-skin co-cultures--A first step toward systemic repeated dose substance testing in vitro. Eur J Pharm Biopharm. 2015; 95:77–87. [PubMed: 25857839]
32. Maschmeyer I, Lorenz AK, Schimek K, Hasenberg T, Ramme AP, Hubner J, et al. A four-organ-chip for interconnected long-term co-culture of human intestine, liver, skin and kidney equivalents. Lab Chip. 2015; 15:2688–99. [PubMed: 25996126]
33. Schweinlin M, Wilhelm S, Schwedhelm I, Hansmann J, Rietscher R, Jurowich C, et al. Development of an Advanced Primary Human In Vitro Model of the Small Intestine. Tissue Eng Part C Methods. 2016; 22:873–83. [PubMed: 27481569]
34. Mahla RS. Stem Cells Applications in Regenerative Medicine and Disease Therapeutics. Int J Cell Biol. 2016; 2016:6940283. [PubMed: 27516776]
35. Miyoshi H, Stappenbeck TS. In vitro expansion and genetic modification of gastrointestinal stem cells in spheroid culture. Nature Protocols. 2013; 8:2471–82. [PubMed: 24232249]
36. Merker SR, Weitz J, Stange DE. Gastrointestinal organoids: How they gut it out. Dev Biol. 2016; 420:239–50. [PubMed: 27521455]
37. In JG, Foulke-Abel J, Estes MK, Zachos NC, Kovbasnjuk O, Donowitz M. Human mini-guts: new insights into intestinal physiology and host-pathogen interactions. Nat Rev Gastroenterol Hepatol. 2016; 13:633–42. [PubMed: 27677718]
38. Zachos NC, Kovbasnjuk O, Foulke-Abel J, In J, Blutt SE, de Jonge HR, et al. Human Enteroids/Colonoids and Intestinal Organoids Functionally Recapitulate Normal Intestinal Physiology and Pathophysiology. J Biol Chem. 2016; 291:3759–66. [PubMed: 26677228]

39. Sato T, Vries RG, Snippert HJ, van de Wetering M, Barker N, Stange DE, et al. Single Lgr5 stem cells build crypt-villus structures in vitro without a mesenchymal niche. Nature. 2009; 459:262–U147. [PubMed: 19329995]
40. Bhatia SN, Ingber DE. Microfluidic organs-on-chips. Nat Biotechnol. 2014; 32:760–72. [PubMed: 25093883]
41. Lancaster MA, Knoblich JA. Organogenesis in a dish: modeling development and disease using organoid technologies. Science. 2014; 345:1247125. [PubMed: 25035496]
42. van de Wetering M, Francies HE, Francis JM, Bounova G, Iorio F, Pronk A, et al. Prospective Derivation of a Living Organoid Biobank of Colorectal Cancer Patients. Cell. 2015; 161:933–45. [PubMed: 25957691]
43. Sato T, Stange DE, Ferrante M, Vries RGJ, van Es JH, van den Brink S, et al. Long-term Expansion of Epithelial Organoids From Human Colon, Adenoma, Adenocarcinoma, and Barrett's Epithelium. Gastroenterology. 2011; 141:1762–72. [PubMed: 21889923]
44. Yin XL, Farin HF, van Es JH, Clevers H, Langer R, Karp JM. Niche-independent high-purity cultures of Lgr5(+) intestinal stem cells and their progeny. Nat Methods. 2014; 11:106–12. [PubMed: 24292484]
45. Liu YW, Gan LH, Carlsson DJ, Fagerholm P, Lagali N, Watsky MA, et al. A simple, cross-linked collagen tissue substitute for corneal implantation. Investigative Ophthalmology & Visual Science. 2006; 47:1869–75. [PubMed: 16638993]
46. Engler, AJ., Rehfeldt, F., Sen, S., Discher, DE. Microtissue elasticity: Measurements by atomic force microscopy and its influence on cell differentiation. In: Wang, YL., Discher, DE., editors. Cell Mechanics. 2007. p. 521-45.
47. Pai JH, Wang Y, Salazar GT, Sims CE, Bachman M, Li GP, et al. Photoresist with low fluorescence for bioanalytical applications. Anal Chem. 2007; 79:8774–80. [PubMed: 17949059]
48. Hu SW, Ren XQ, Bachman M, Sims CE, Li GP, Allbritton N. Surface modification of poly(dimethylsiloxane) microfluidic devices by ultraviolet polymer grafting. Analytical Chemistry. 2002; 74:4117–23. [PubMed: 12199582]
49. Yang CR. Enhanced physicochemical properties of collagen by using EDC/NHS-crosslinking. Bull Mat Sci. 2012; 35:913–8.
50. Vrana NE, Builles N, Kocak H, Gulay P, Justin V, Malbouyres A, et al. EDC/NHS cross-linked collagen foams as scaffolds for artificial corneal stroma. J Biomater Sci-Polym Ed. 2007; 18:1527–45. [PubMed: 17988518]
51. Schuijers J, van der Flier LG, van Es J, Clevers H. Robust Cre-Mediated Recombination in Small Intestinal Stem Cells Utilizing the Olfm4 Locus. Stem Cell Reports. 2014; 3:234–41. [PubMed: 25254337]
52. Van der Flier LG, Haegebarth A, Stange DE, Van de Wetering M, Clevers H. OLFM4 Is a Robust Marker for Stem Cells in Human Intestine and Marks a Subset of Colorectal Cancer Cells. Gastroenterology. 2009; 137:15–7. [PubMed: 19450592]
53. Szpak P. Fish bone chemistry and ultrastructure: implications for taphonomy and stable isotope analysis. J Archaeol Sci. 2011; 38:3358–72.
54. Louvard D, Kedinger M, Hauri HP. The differentiating intestinal epithelial cell: establishment and maintenance of functions through interactions between cellular structures. Annu Rev Cell Biol. 1992; 8:157–95. [PubMed: 1476799]
55. Beaulieu JF. Differential expression of the VLA family of integrins along the crypt-villus axis in the human small intestine. J Cell Sci. 1992; 102:427–36. [PubMed: 1506425]
56. Atuma C, Strugala V, Allen A, Holm L. The adherent gastrointestinal mucus gel layer: thickness and physical state in vivo. American Journal of Physiology-Gastrointestinal and Liver Physiology. 2001; 280:G922–G9. [PubMed: 11292601]
57. Ulluwishewa D, Anderson RC, McNabb WC, Moughan PJ, Wells JM, Roy NC. Regulation of Tight Junction Permeability by Intestinal Bacteria and Dietary Components. J Nutr. 2011; 141:769–76. [PubMed: 21430248]
58. VanDussen KL, Carulli AJ, Keeley TM, Patel SR, Puthoff BJ, Magness ST, et al. Notch signaling modulates proliferation and differentiation of intestinal crypt base columnar stem cells. Development. 2012; 139:488–97. [PubMed: 22190634]

59. Olsauskas-Kuprys R, Zlobin A, Osipo C. Gamma secretase inhibitors of Notch signaling. Oncotargets and Therapy. 2013; 6:943–55. [PubMed: 23901284]
60. van Es JH, van Gijn ME, Riccio O, van den Born M, Vooijs M, Begthel H, et al. Notch/gamma-secretase inhibition turns proliferative cells in intestinal crypts and adenomas into goblet cells. Nature. 2005; 435:959–63. [PubMed: 15959515]
61. Cayo MA, Cayo AK, Jarjour SM, Chen H. Sodium butyrate activates Notch1 signaling, reduces tumor markers, and induces cell cycle arrest and apoptosis in pheochromocytoma. American Journal of Translational Research. 2009; 1:178–83. [PubMed: 19956429]
62. Davie JR. Inhibition of histone deacetylase activity by butyrate. J Nutr. 2003; 133:2485S–93S. [PubMed: 12840228]
63. Benjamin J, Makharia G, Ahuja V, Rajan KDA, Kalaivani M, Gupta SD, et al. Glutamine and Whey Protein Improve Intestinal Permeability and Morphology in Patients with Crohn's Disease: A Randomized Controlled Trial. Dig Dis Sci. 2012; 57:1000–12. [PubMed: 22038507]
64. Attayek PJ, Ahmad AA, Wang Y, Williamson I, Sims CE, Magness ST, et al. In Vitro Polarization of Colonoids to Create an Intestinal Stem Cell Compartment. PLoS One. 2016; 11:e0153795. [PubMed: 27100890]
65. Heath JP. Epithelial cell migration in the intestine. Cell Biol Int. 1996; 20:139–46. [PubMed: 8935158]
66. Moutairou K, Fritsch P, Meslin JC, Poncy JL, Metivier H, Masse R. Epithelial cell migration on small intestinal villi in the neonatal rat. Comparison between [3H] thymidine and cytoplasmic labelling after Pu-citrate ingestion. Biol Cell. 1989; 65:265–9. [PubMed: 2665887]
67. Lai YZ, Asthana A, Kisaalita WS. Biomarkers for simplifying HTS 3D cell culture platforms for drug discovery: the case for cytokines. Drug Discovery Today. 2011; 16:293–7. [PubMed: 21277382]
68. Wypych, G. Handbook of Polymers. Toronto ChemTec Publishing; 2012.
69. Fuard D, Tzvetkova-Chevolleau T, Decossas S, Tracqui P, Schiavone P. Optimization of poly-di-methyl-siloxane (PDMS) substrates for studying cellular adhesion and motility. Microelectronic Engineering. 2008; 85:1289–93.
70. Kim HJ, Li H, Collins JJ, Ingber DE. Contributions of microbiome and mechanical deformation to intestinal bacterial overgrowth and inflammation in a human gut-on-a-chip. Proceedings of the National Academy of Sciences of the United States of America. 2016; 113:E7–E15. [PubMed: 26668389]
71. Costello CM, Jia HP, Shaffiey S, Yu JJ, Jain NK, Hackam D, et al. Synthetic Small Intestinal Scaffolds for Improved Studies of Intestinal Differentiation. Biotechnology and Bioengineering. 2014; 111:1222–32. [PubMed: 24390638]
72. Shaffiey SA, Jia HP, Keane T, Costello C, Wasserman D, Quidgley M, et al. Intestinal stem cell growth and differentiation on a tubular scaffold with evaluation in small and large animals. Regenerative Medicine. 2016; 11:45–61. [PubMed: 26395928]
73. Jabaji Z, Sears CM, Brinkley GJ, Lei NY, Joshi VS, Wang J, et al. Use of collagen gel as an alternative extracellular matrix for the in vitro and in vivo growth of murine small intestinal epithelium. Tissue Eng Part C Methods. 2013; 19:961–9. [PubMed: 23566043]
74. Jabaji Z, Brinkley GJ, Khalil HA, Sears CM, Lei NY, Lewis M, et al. Type I Collagen as an Extracellular Matrix for the In Vitro Growth of Human Small Intestinal Epithelium. PLoS One. 2014:9.
75. DuFort CC, Paszek MJ, Weaver VM. Balancing forces: architectural control of mechanotransduction. Nature Reviews Molecular Cell Biology. 2011; 12:308–19. [PubMed: 21508987]
76. Sung JH, Yu JJ, Luo D, Shuler ML, March JC. Microscale 3-D hydrogel scaffold for biomimetic gastrointestinal (GI) tract model. Lab on a Chip. 2011; 11:389–92. [PubMed: 21157619]

Appendix A. Supplementary data

Table S1. Supplier, catalog number, stock solution concentration, and storage condition of reagents

Table S2. Formulation of culture media for small intestinal epithelial cells

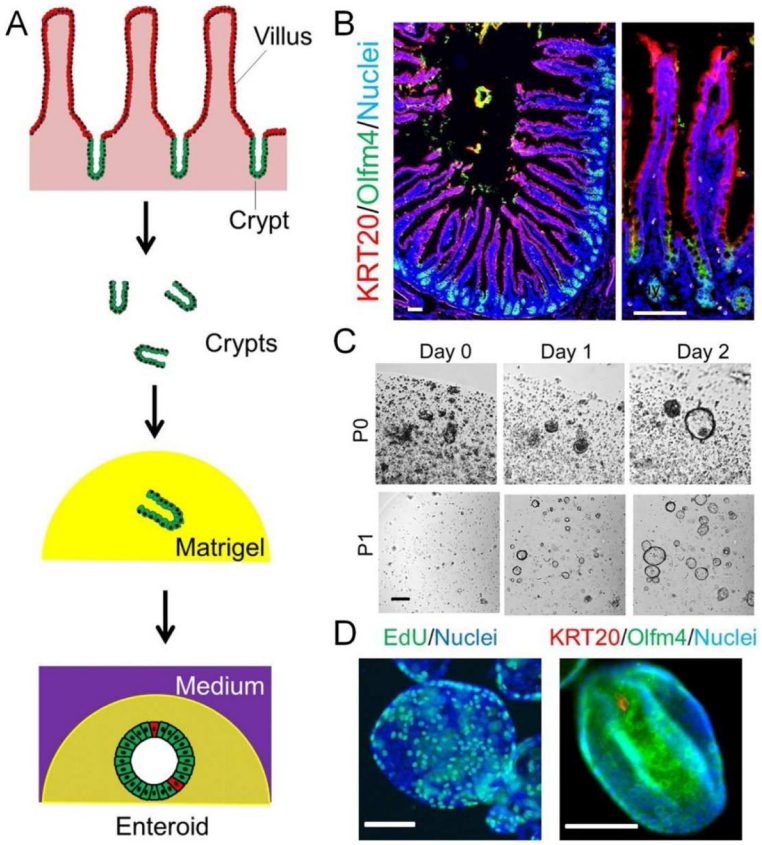

Fig. 1.

The enteroid culture system converts the highly structured *in vivo* crypt-villus architecture into non-polarized enteroids with an inaccessible lumen. (A) Schematic showing the isolation crypts from human small intestinal mucosa and their culture as enteroids. Stem and progenitor cells are green while differentiated cells are red. (B) Immunofluorescence staining of freshly obtained human small intestinal tissues showing that the epithelium is composed of an array of crypts/villi with differentiated cells ($KRT20^{+}$) located along the villi while the stem and progenitor cells are confined within the crypts ($Olfm4^{+}$). DNA (nuclei) was stained with Hoechst 33342. (C) Enteroid culture of human small intestine crypts by embedding in Matrigel. Shown are the structures on day 0, 1, and 2 of culture at passage number 0 and 1. (D) EdU and immunofluorescence staining of human enteroids after 4 days in culture. Scale bar = 100 μm.

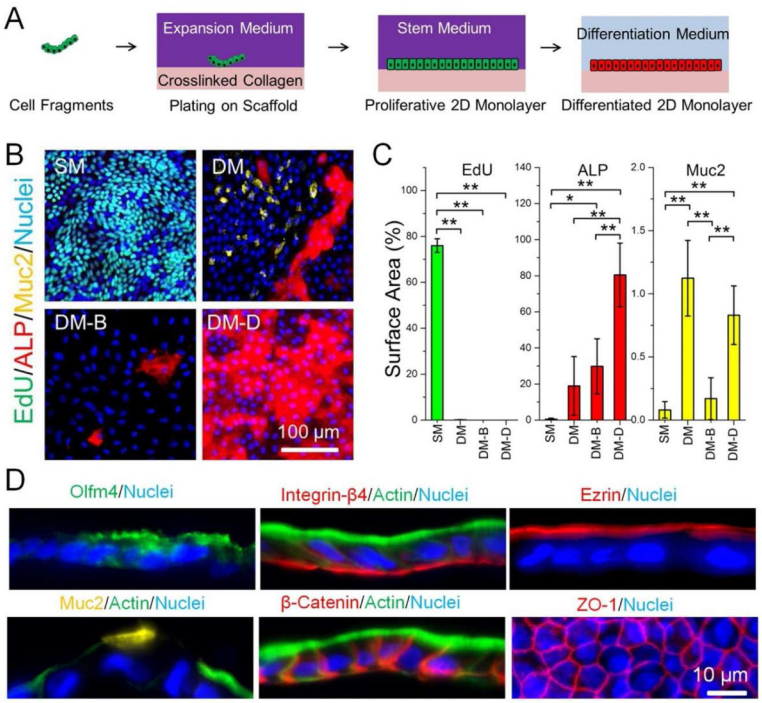

Fig. 2.

Monolayer culture of human small intestinal cells on a cross-linked collagen hydrogel. (A) Schematic of the culture of cells on the cross-linked collagen followed by forced differentiation of the cells. (B) Cells were cultured in expansion medium (EM, 4 days) and then either stem medium (SM) or differentiation medium (DM) for 4 days. Additional reagents added to the differentiation media 5 mM butyrate (DM-B) or 10 μM DAPT (DM-D). Colors as follows: EdU, green; ALP, red; Muc2, yellow; DNA, blue. (C) The percentage of the monolayer surface area displaying fluorescence from the EdU, Muc2, and ALP stains under the various culture conditions. (D) Monolayer side view of Oflm4 (SM), integrin-β4 and actin (DM), ezrin (DM), Muc2 (DM), β-catenin and actin (DM), and top view of ZO-1 (DM). DNA (nuclei) was stained with Hoechst 33342.

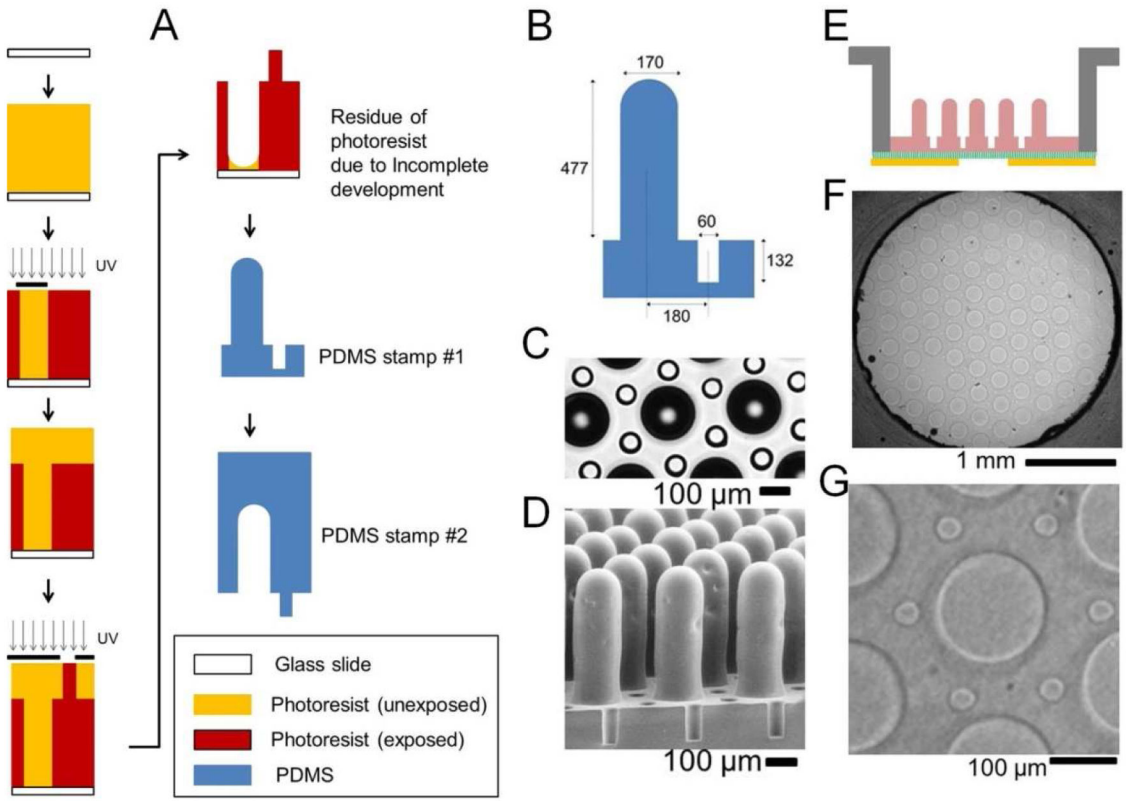

Fig. 3.

Micromolding a collagen scaffold on a porous membrane. (A) Schematic of the process used to generate the PDMS stamp to micromold the collagen. (B) The dimensions of microstructures in stamp #1 which replicate the features formed in the collagen. The units for the numbers are in µm. (C) A top view of stamp #1 is shown using brightfield microscopy. (D) A side view of stamp #1 is shown using electron microscopy. (E) Schematic of micromolded collagen in the modified insert. (F) Top views of the shaped collagen array acquired by brightfield microscopy. (G) A close-up view.

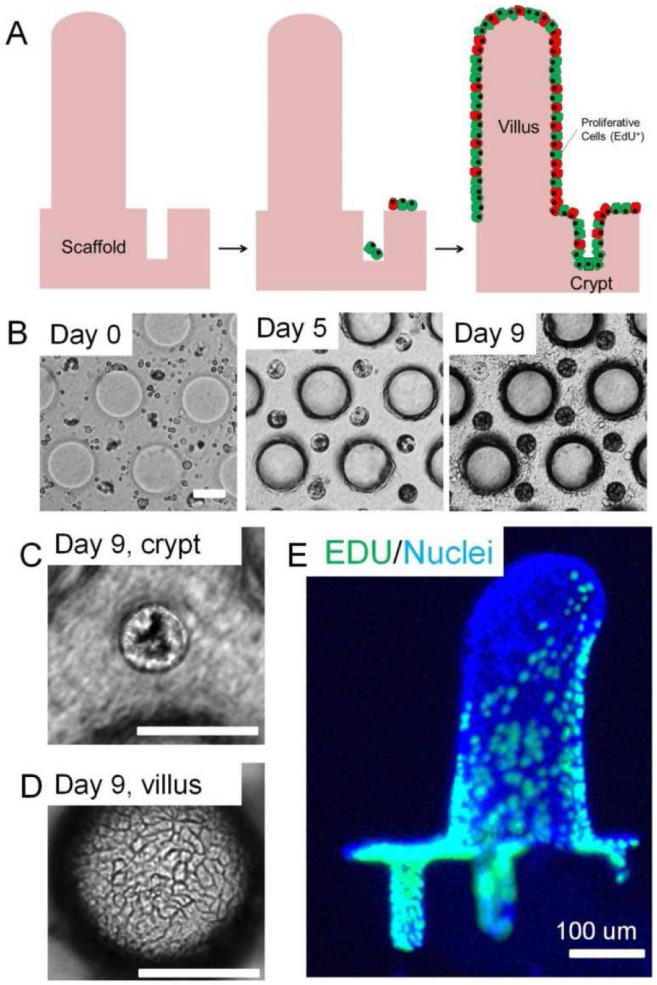

Fig. 4.

Culture of human small intestinal cells on a collagen scaffold recreates *in vitro* crypt-villus architecture. (A) Schematic of cell propagation on the microstructures. (B) Cells cultured on a scaffold were tracked by brightfield microscopy over time as the cells spread across the scaffold surface. (C) A brightfield image with the focal plane at the level of the crypt showing that cells migrated into the microwell. (D) An image with the focal plane at the top of the villus showing cells migrated to the top of the micropillar. (E) Fluorescence side view image of the crypt-villus architecture displaying one villus and two crypt structures from an EdU-pulsed array.

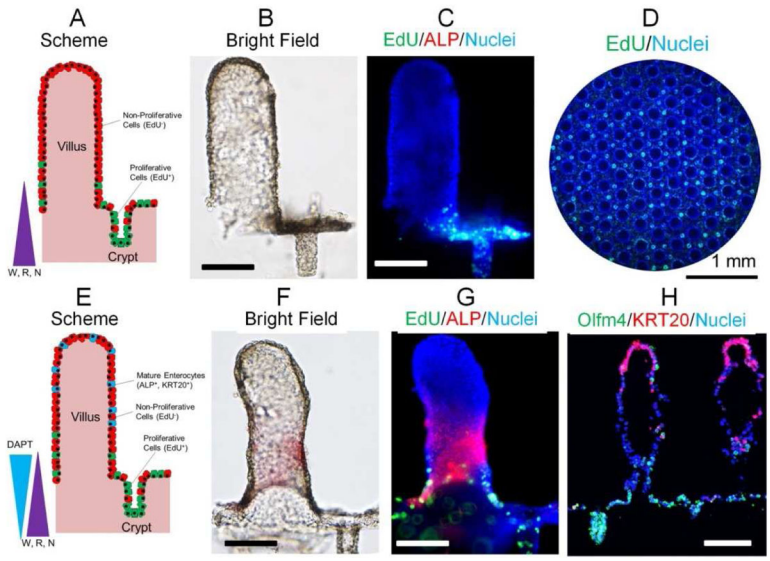

Fig. 5.

Creating a polarized tissue by applying gradients to the *in vitro* crypt-villus arrays. (A) Schematic of the gradient of growth factors (W: Wnt-3A; R: R-spondin 3; N: noggin). Brightfield (B) and fluorescence (C) images of a polarized crypt-villus unit under the 3-growth factor gradient. EdU^+ cells (green) are confined to the crypt and adjacent regions, while no ALP^+ cells (red) are observed. DNA or nuclei are shown in blue. (D) A wide field view of the polarized crypt-villus epithelium array (3 mm in diameter) under the 3-growth factor gradient. (E) Schematic showing the application of an additional gradient comprised of DAPT (gamma secretase inhibitor). Brightfield (F) and fluorescence (G) images of a polarized crypt-villus unit under the 3-growth factor gradient and opposing DAPT gradient. Mature enterocytes (red, ALP^+) and proliferative cells (green, EdU^+) are also marked. (H) Immunofluorescence staining (Olfm4/KRT20) of *in vitro* human small intestinal tissues showing tissue polarity under the combine growth factor and DAPT gradient. Scale bar = 100 μm for B,C,F,G,H.

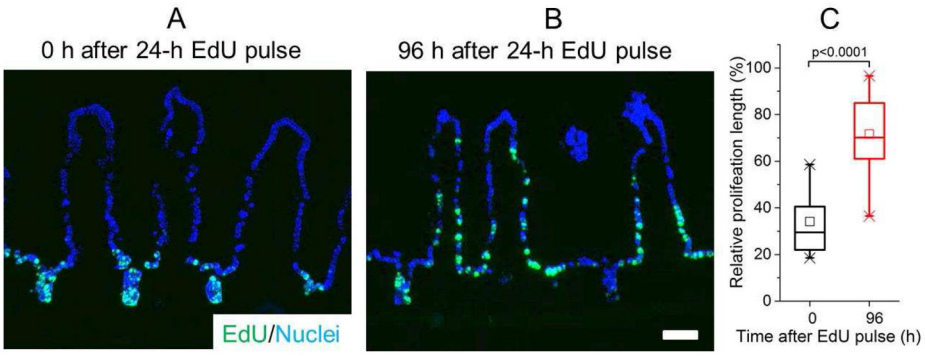

Fig. 6.

Cell migration up the crypt-villus axis of the *in vitro* tissue over time. Tissues were fixed at 0 (A) and 96 (B) h post-EdU pulse (24-h EdU pulse duration), and the incorporated EdU was labeled with an EdU-reactive Alex Fluor dye (green). DNA or nuclei were stained with Hoechst 33342 (blue) (C) Box plots of the relative proliferation length which was defined as the length of EdU^+ tissue divided by the cypt + villus length (659 μm) at 0 and 96 h post-EdU pulse. 26 (0 h) and 20 (96 h) crypt-villus units were quantified. $p<0.0001$ based on t-test. Scale bar = 100 μm